

# Spherical Gerotor: Synthesis of a Novel Valveless Pulsatile Flow Spherical Total Artificial Heart

Mengtang Li and Eric J. Barth

*Department of Mechanical Engineering, Vanderbilt University, 2301 Vanderbilt Place, Nashville, TN 37235, USA*

**Abstract:** Though mechanical circulatory support (MCS) devices, such as ventricular assist device (VAD) and total artificial heart (TAH), indeed provide heart failure patients with an alternative to transplantation, many complications are provided at the same time due to the non-pulsatile blood flow or high blood shear induced by those MCS. A novel spherical total artificial heart (TAH) based on the concept of hydraulic gerotor pump is proposed. This spherical TAH features volumetric pumping mechanism, pulsatile flow generating and low blood shear. It consists of four time-varying chambers partitioned by two orange shape wedges and one complex curve cut disk. The disk rotates as twice fast as the wedges, while all in the same direction. The TAH sucks in and pumps out blood through four ports located at the pump peripheral. This paper presents the fundamental equations which establish the geometric shape of the TAH, develop the range of the size specs, and show the analytical model for the time-varying chamber volume.

**Key words:** TAH, spherical gerotor, design.

## I. Introduction

Heart failure has a prevalence of 1.7 in 100 persons globally [1, 2], with the number of patients expected to grow by 50% over the next 15 years [3, 4]. For end stage cases, surgical transplantation of a healthy heart from a donor requires a group of surgeries lasting several hours, a post-operative ICU stay and significant potential morbidity and discomfort. While this surgery does offer an effective way to overcome heart failure and the number of heart transplants worldwide has reached at approximately 5,000 in 2016, only twenty percent of the patient population are fortunate enough to receive heart transplant and waiting list is the life destination for a considerable number of unfortunate patients [5-9]. Though mechanical circulatory support (MCS) devices, such as ventricular assist device (VAD) and total artificial heart (TAH), indeed provide heart failure patients with a bridge to eventual heart transplantation or an

alternative to transplantation [10], many complications, such as aortic insufficiency [11-13], thromboembolic complications [14, 15], gastrointestinal bleeding [16-18] and impaired renal function [19, 20], are provided at the same time due to the non-pulsatile blood flow or high blood shear induced by those MCSs [21]. Those complications can also be the consequences of mechanical heart valves (MHV) [4]. The high prevalence of heart failure and the lifelong anticoagulation needs as a consequence of current MCS implantation motivate a novel TAH design.

In Section 2, a brief review of current TAH and VAD is presented, with their pros and cons discussed. Next, the fundamental working principle of the proposed spherical gerotor based TAH pump, along with the advantages of the hydraulic gerotor pump, is presented in Section 3.1. Methods to derive the geometry shape of the spherical gerotor pump are described in details in Sections 3.3 and 3.4. Section 3.5 follows and establishes an analytical model to calculate the chamber volume with respect to rotated angle. A discussion follows in Section 4. Section 5 provides concluding remarks.

---

**Corresponding author:** Mengtang Li, M.S. in Electrical Engineering and M.S. in Mechanical Engineering, research fields: hydraulic power system, soft robot, mechanical circulatory system.

## 2. Brief Review of Current TAH and VAD

Most of the current TAH pumps and VADs can be generally classified into (in the manner of hydraulics terms) positive displacement pump and non-positive displacement pump [22]. A positive displacement TAH pump usually consists of a reciprocating piston or a membrane driven by controlled pneumatic air (e.g. SynCardia) or hydraulic oils (e.g. Carmat) on the other side. With the aid of MHVs, those pumps are able to generate pulsatile blood flow like the real one. Yet, the usage of elastic membranes limits the durability, the overall size requires bulky space [23, 24] and the involvement of four valves increases the device thrombogenicity. Most of the current VADs and some TAHs are continuous flow pumps, which usually utilize a magnetically levitated impeller (e.g. BiVACOR, HeartMate 3). Compared with the previous type, they are more durable, much smaller, and require no valve. However, the output flow of these non-positive displacement pumps is pressure dependent [23]. And non-pulsatile blood flow induces many complications [21]. Another type of TAH is to mimic the real one [25], though even the current state of the art material does not allow a long time of massive deformation. Two recent designs are interesting and deserve more research. A rotary piston blood pump, adopting the architecture of a vehicle rotary engine, combines the benefits of membrane

pump and rotary pump [26]. Another one, which is similar to our concept, is a spherical shape TAH with four chambers divided by two rotating disks [27].

## 3. Method

### 3.1 Device Description

The proposed novel spherical gerotor is inspired by the hydraulic gerotor pump, which is among the most common pump architectures in fluid power systems. Compared with other rotary positive displacement pumps (e.g. external gear pump, axial impeller pump), both the inner and outer rotors of a gerotor pump rotate together, which leads to dramatically lower shear stress since the velocity gradient is much smaller. A gerotor core is shown in Fig. 1a with a 8-tooth inner gear and a 9-tooth outer gear, and another gerotor core with a 2-tooth inner gear and a 3-tooth outer gear is shown in Fig. 1b. Note that there is an eccentricity between the inner gear and outer gear. Since the inner and outer gears have different number of teeth, the rotation speeds are also different, causing the volumes of those chambers partitioned by those gear teeth vary cyclically.

The spherical gerotor TAH pump consists of four time-varying chambers partitioned by two wedges and one rotating disk. For the sake of concept illustration, the two-chamber version is presented here first. As shown in Fig. 2a, the wedge rotates along its own

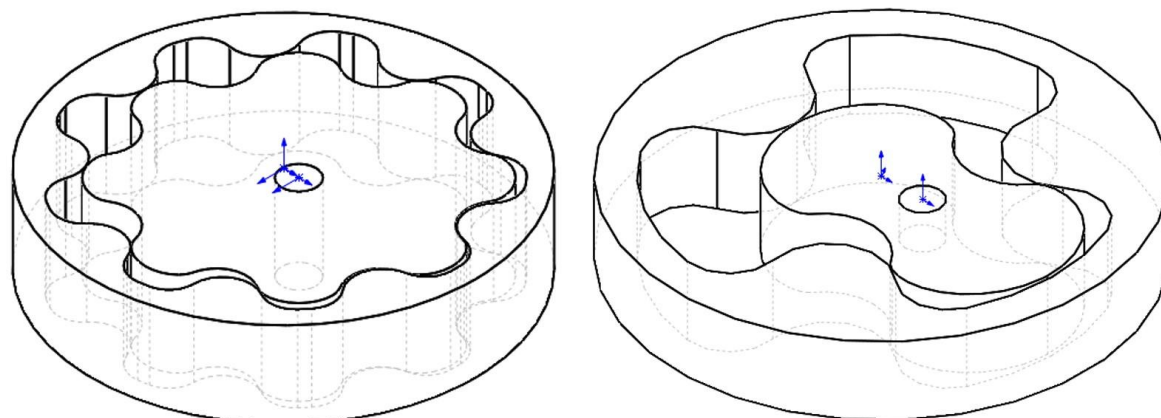
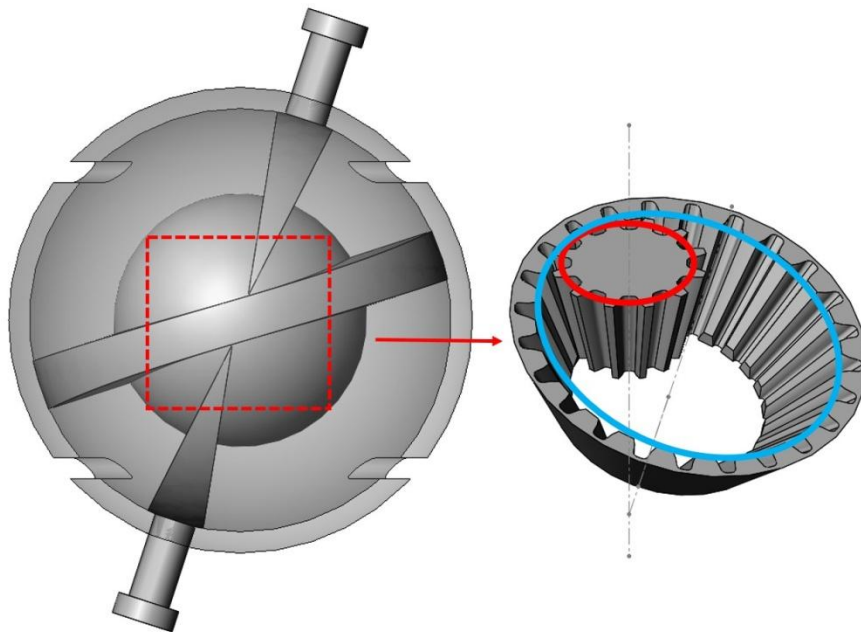


Fig. 1 (a) A gerotor core with 8-tooth inner gear and 9-tooth outer gear; (b) a gerotor core with 2-tooth inner gear and 3-tooth outer gear.



**Fig. 2** (a) A 4-chamber version of the spherical gerotor TAH; (b) the inner bevel gear set.

axial axis through the center of the sphere and the semi-sphere part rotates along a virtual vertical axis with twice the speed of the wedge, which is realized through a customized designed bevel gear set with 1:2 gear ratio as shown in Fig. 2b. The overall system has only 1 degree of freedom now and rotation of the wedge entrains the rotation of the semi-sphere, causing the volumes of the two chambers to vary cyclically. The device working principle is further illustrated in Fig. 3. Two chambers are partitioned by the wedge, namely *Ch1* and *Ch2*. At the beginning, *Ch1* reaches the minimum volume and *Ch2* reaches the maximum volume. As the wedge is rotating with respect to its own axial axis through the center of the sphere in the right-hand direction, the volume of *Ch1* is increasing while that of *Ch2* is decreasing. When the rotated angle equals to  $\pi$ , *Ch1* reaches the maximum and the *Ch2* reaches the minimum. After  $\pi$  as the rotation continued, the volume of *Ch1* is decreasing while that of *Ch2* is increasing. A complete cycle is finished once the wedge rotates  $2\pi$  and the semi-sphere rotates  $4\pi$ .

### 3.2 Shape Design

The most significant part of the novel spherical

gerotor design is the geometry of the seemingly semi-sphere which allows the sliding contact between the wedge and the semi-sphere. As it will be shown here through the kinematic equations, the seemingly semi-sphere has a complex shape and it is little different between the 2-chamber version and the 4-chamber version.

### 3.3 2-Chamber Version

Simple angle constraints are considered first before deriving the actual kinematic equations of the wedge. Intuitively, since the 1:2 gear ratio, when the wedge rotates  $wt = \pi/2$ , the semi-sphere rotates  $2wt = \pi$ . Fig. 4a shows a front view for the spherical gerotor at  $wt = 0$  and Fig. 4b shows the front view at  $wt = \pi/2$ . The angle constraints are then

$$\alpha < \beta = \gamma \quad (1)$$

To derive the kinematic equations of the two tips of the wedge and therefore the geometry of the semi-sphere, the bevel gear set of Fig. 2b is treated as a planetary gear set shown in Fig. 5. The pinion gear (red in Figs. 2b and 5) is fixed as the sun and the bevel gear (blue in Figs. 2b and 5) is rotating as the planet. The following geometry relationships exist:

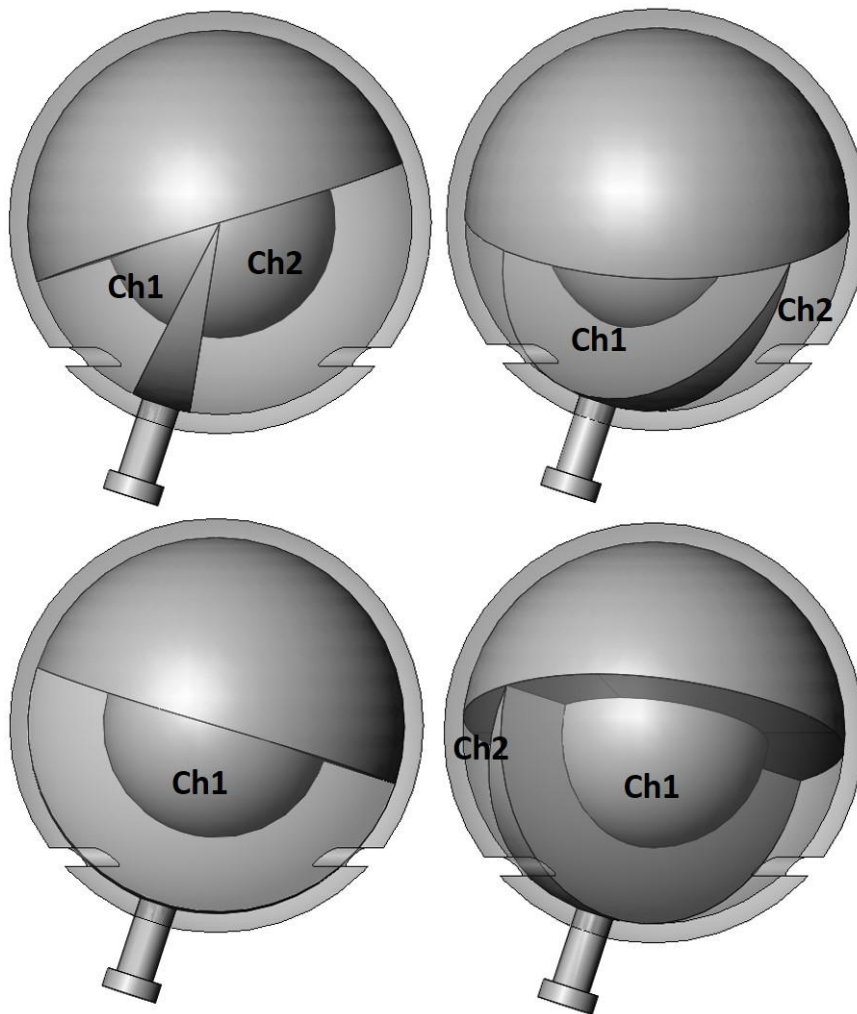


Fig. 3 Working principle: (a) rotated angle  $wt = 0 \text{ rad}$ , (b) rotated angle  $wt = \pi/4 \text{ rad}$ , (c) rotated angle  $wt = \pi/2 \text{ rad}$ , (d) rotated angle  $wt = 3\pi/2 \text{ rad}$ .

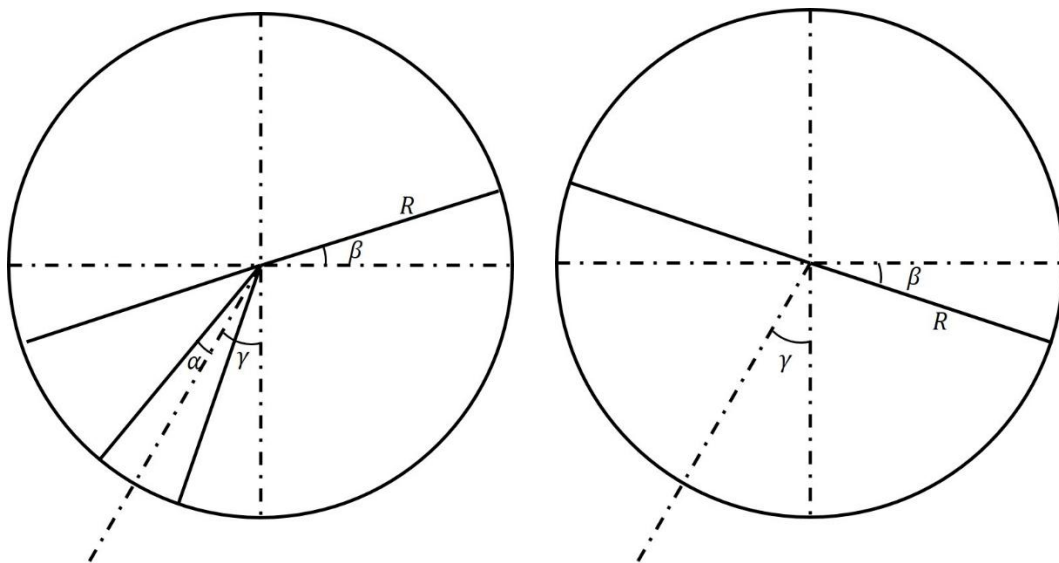


Fig. 4 Working principle: (a) front view at rotated angle  $wt = 0 \text{ rad}$ . (b) front view at rotated angle  $wt = \pi/2 \text{ rad}$ .

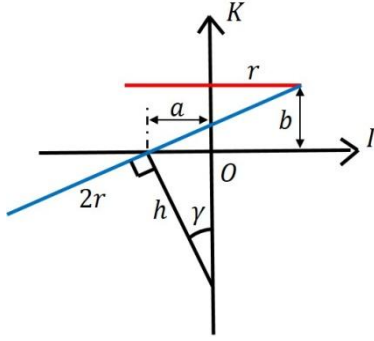


Fig. 5 Front view of the planetary gear set.

$$h = r \frac{2 \cos \gamma - 1}{\sin \gamma} \quad (2)$$

$$a = h \sin \gamma = r(2 \cos \gamma - 1) \quad (3)$$

$$b = 2r \sin \gamma \quad (4)$$

Three frames are introduced to ease the kinematic equation derivation, shown in Fig. 6. The first inertial frame,  $IJK$ , is fixed at the origin  $O$ . The center of the second one, a local frame  $ijk$ , is rotating on the  $IJ$ -plane at a speed of  $2w$  with a radius of  $a$ . Its  $i$ -axis and  $j$ -axis lie in the bevel gear plane and its  $k$ -axis perpendicular to the bevel gear. In order for the two gears to rotate correctly, meaning no slip between the red and blue cycles in Fig. 2b, the third frame, another local frame  $xyz$ , is rotating with a speed of  $-w$ . Its  $z$ -axis coincides with the  $k$ -axis. The transformation matrices below allow the conversion of the local coordinates  $xyz$  to global inertial coordinates  $IJK$ . For the sake of space,  $c(\cdot)$  and  $s(\cdot)$  represent  $\cos(\cdot)$  and  $\sin(\cdot)$  respectively.

$$R_1 \begin{bmatrix} \bar{i} \\ \bar{j} \\ \bar{k} \end{bmatrix} = \begin{bmatrix} c\beta c(2wt) & -s(2wt) & -s\beta c(2wt) \\ c\beta s(2wt) & c(2wt) & -s\beta s(2wt) \\ s\beta & 0 & c\beta \end{bmatrix} \begin{bmatrix} \bar{i} \\ \bar{j} \\ \bar{k} \end{bmatrix} \quad (5)$$

$$= \begin{bmatrix} \bar{I} \\ \bar{J} \\ \bar{K} \end{bmatrix}$$

$$R_2 \begin{bmatrix} \bar{x} \\ \bar{y} \\ \bar{z} \end{bmatrix} = \begin{bmatrix} c(-wt) & -s(-wt) & 0 \\ s(-wt) & c(-wt) & 0 \\ 0 & 0 & 1 \end{bmatrix} \begin{bmatrix} \bar{x} \\ \bar{y} \\ \bar{z} \end{bmatrix} = \begin{bmatrix} \bar{i} \\ \bar{j} \\ \bar{k} \end{bmatrix} \quad (6)$$

$$R_3 \begin{bmatrix} \bar{x} \\ \bar{y} \\ \bar{z} \end{bmatrix} = R_1 R_2 \begin{bmatrix} \bar{x} \\ \bar{y} \\ \bar{z} \end{bmatrix} = \begin{bmatrix} \bar{I} \\ \bar{J} \\ \bar{K} \end{bmatrix} \quad (7)$$

The distance between the global origin and the center of bevel gear is

$$\bar{R} = -hs\beta c(2wt)\bar{I} - hs\beta s(2wt)\bar{J} + 0\bar{K} \quad (8)$$

The local coordinates for the two tips on the wedge are simply two points on a circle:

$$\bar{\rho}_1 = \begin{bmatrix} 2rc(\frac{\pi}{2}) & 2rs(\frac{\pi}{2}) & 0 \end{bmatrix} \begin{bmatrix} \bar{x} \\ \bar{y} \\ \bar{z} \end{bmatrix} \quad (9)$$

$$= \begin{bmatrix} 2rc(\frac{\pi}{2}) & 2rs(\frac{\pi}{2}) & 0 \end{bmatrix} R_3^{-1} \begin{bmatrix} \bar{I} \\ \bar{J} \\ \bar{K} \end{bmatrix}$$

$$\bar{\rho}_2 = \begin{bmatrix} 2rc(\frac{3\pi}{2}) & 2rs(\frac{3\pi}{2}) & 0 \end{bmatrix} \begin{bmatrix} \bar{x} \\ \bar{y} \\ \bar{z} \end{bmatrix} \quad (10)$$

$$= \begin{bmatrix} 2rc(\frac{3\pi}{2}) & 2rs(\frac{3\pi}{2}) & 0 \end{bmatrix} R_3^{-1} \begin{bmatrix} \bar{I} \\ \bar{J} \\ \bar{K} \end{bmatrix}$$

The global coordinates for the two tips on the wedge are then

$$\bar{r}_1 = \bar{R} + \bar{\rho}_1 \quad (11)$$

$$\bar{r}_2 = \bar{R} + \bar{\rho}_2 \quad (12)$$

Note that the transformation matrices  $R_1$ ,  $R_2$ ,  $R_3$  are time varying, so  $\bar{r}_1$ ,  $\bar{r}_2$  will give the trajectories (blue dash line) of the two tips of the wedge (blue solid line), which of course are the same one, shown in Fig. 7. Remember that the gear set is treated as a planetary gear set for the sake of derivation easiness. To get the actual trajectory, both of the gears should rotate which means the center of the wedge should be moved to the global origin and the radius of the spherical gerotor, instead of the gear, should be used here. The local coordinates of the two tips on the wedge are:

$$\bar{\rho}'_1 = \begin{bmatrix} Rc(\frac{\pi}{2}) & Rs(\frac{\pi}{2}) & -h \end{bmatrix} \begin{bmatrix} \bar{x} \\ \bar{y} \\ \bar{z} \end{bmatrix} \quad (13)$$

$$= \begin{bmatrix} Rc(\frac{\pi}{2}) & Rs(\frac{\pi}{2}) & -h \end{bmatrix} R_3^{-1} \begin{bmatrix} \bar{I} \\ \bar{J} \\ \bar{K} \end{bmatrix}$$

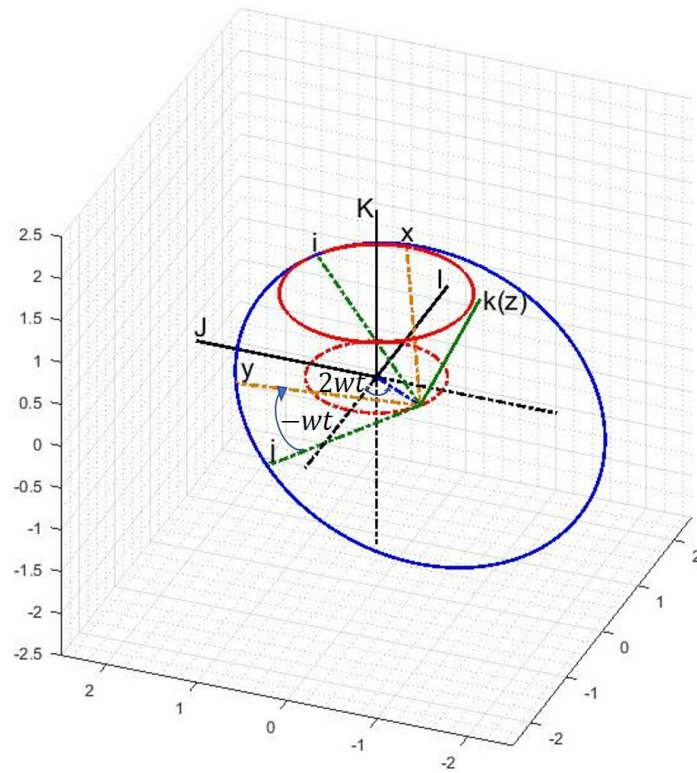


Fig. 6 Transformation matrices.

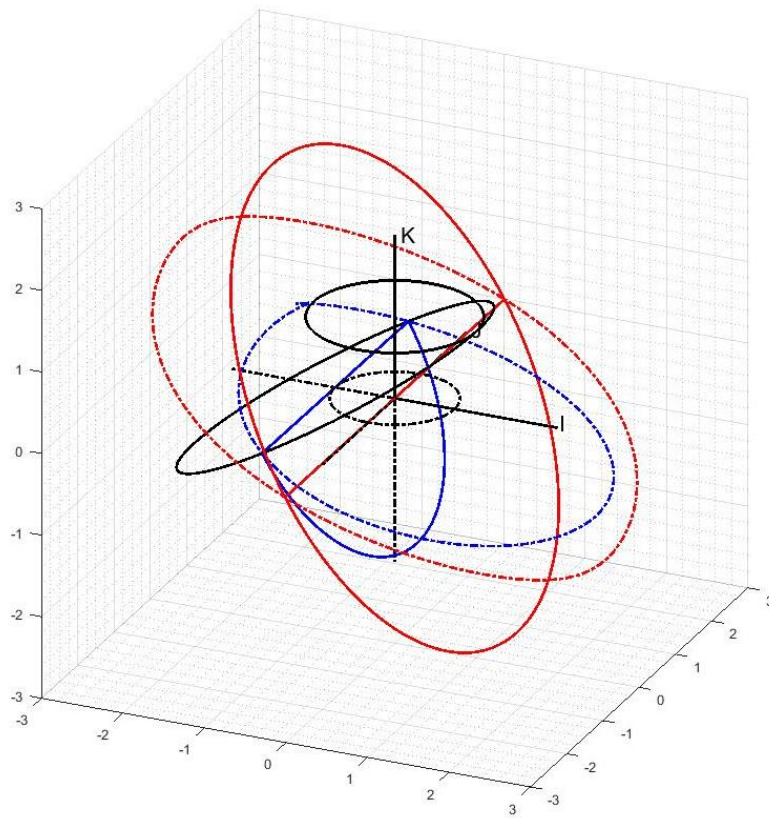


Fig. 7 Trajectories for the two tips on the wedge.

$$\begin{aligned}\bar{\rho}'_2 &= \begin{bmatrix} Rc(\frac{3\pi}{2}) & Rs(\frac{3\pi}{2}) & -h \end{bmatrix} \begin{bmatrix} \bar{x} \\ \bar{y} \\ \bar{z} \end{bmatrix} \\ &= \begin{bmatrix} Rc(\frac{3\pi}{2}) & Rs(\frac{3\pi}{2}) & -h \end{bmatrix} R_3^{-1} \begin{bmatrix} \bar{I} \\ \bar{J} \\ \bar{K} \end{bmatrix}\end{aligned}\quad (14)$$

The global coordinates for the two tips on the wedge are then

$$\bar{r}'_1 = \bar{R} + \bar{\rho}'_1 + h \cos \beta \bar{K} \quad (15)$$

$$\bar{r}'_2 = \bar{R} + \bar{\rho}'_2 + h \cos \beta \bar{K} \quad (16)$$

The actual trajectory of wedge of the spherical gerotor is obtained and is shown with red dash line in Fig. 7. A surface defined by this trajectory allows smooth contact between the wedge and the seemingly semi-sphere part.

$$\bar{\rho}''_1 = \begin{bmatrix} Rc(\frac{\pi}{2})c\theta & Rs(\frac{\pi}{2})c\theta & Rs\theta - h \end{bmatrix} R_3^{-1} \begin{bmatrix} \bar{I} \\ \bar{J} \\ \bar{K} \end{bmatrix} \quad (18)$$

$$\bar{\rho}''_2 = \begin{bmatrix} Rc(\frac{\pi}{2})c(\pi - \theta) & Rs(\frac{\pi}{2})c(\pi - \theta) & Rs(\pi - \theta) - h \end{bmatrix} R_3^{-1} \begin{bmatrix} \bar{I} \\ \bar{J} \\ \bar{K} \end{bmatrix} \quad (19)$$

$$\bar{\rho}''_3 = \begin{bmatrix} Rc(\frac{\pi}{2})c(\pi + \theta) & Rs(\frac{\pi}{2})c(\pi + \theta) & Rs(\pi + \theta) - h \end{bmatrix} R_3^{-1} \begin{bmatrix} \bar{I} \\ \bar{J} \\ \bar{K} \end{bmatrix} \quad (20)$$

$$\bar{\rho}''_4 = \begin{bmatrix} Rc(\frac{\pi}{2})c(2\pi - \theta) & Rs(\frac{\pi}{2})c(2\pi - \theta) & Rs(2\pi - \theta) - h \end{bmatrix} R_3^{-1} \begin{bmatrix} \bar{I} \\ \bar{J} \\ \bar{K} \end{bmatrix} \quad (21)$$

The global coordinates of them are then

$$\bar{r}''_1 = \bar{R} + \bar{\rho}''_1 + hc\beta\bar{K} \quad (22)$$

$$\bar{r}''_2 = \bar{R} + \bar{\rho}''_2 + hc\beta\bar{K} \quad (23)$$

$$\bar{r}''_3 = \bar{R} + \bar{\rho}''_3 + hc\beta\bar{K} \quad (24)$$

$$\bar{r}''_4 = \bar{R} + \bar{\rho}''_4 + hc\beta\bar{K} \quad (25)$$

The actual trajectories of the two wedges of the 4-chamber spherical gerotor are obtained and are shown with red dash line in Fig. 9. Two surfaces defined by these trajectories allow smooth contact between the upper and lower wedges and the middle disk part.

### 3.5 Time-Varying Volume

As the working principle of this novel spherical

### 3.4 4-Chamber Version

The above design can be extended a little further to contain four chambers in one single sphere. The surface defined above should be modified. Simply mirroring another wedge part to the upper side will not work because that would require an infinite thin piece to separate the upper and lower side. A front view of the 4-chamber spherical gerotor at  $wt = 0$  is shown in Fig. 8a and a side view of the modified wedge is shown in Fig. 8b. The following geometry relationship exists:

$$d = Rs\theta \quad (17)$$

Similar to Eqs. (13) and (14), the local coordinates of the four tips on the upper modified wedge and the two tips on the lower modified wedge respectively are:

gerotor TAH is only briefly introduced in section 2, an analytical model for the time-varying volume of each chamber is developed in this section to better describe the pump behavior, shown in Fig. 10. The complex surface mathematically defined above is treated as an infinite thin circular surface to derive the chamber volume. The assumption is solid once the wedge modified distance  $d$  is small and tilt angle  $\gamma$  is not too big. Noting that the volume of each chamber at every position is a portion of the whole sphere, the volume can be expressed as

$$V = \frac{\psi}{2\pi} \cdot \frac{4}{3}\pi(R^3 - R_s^3) \quad (26)$$

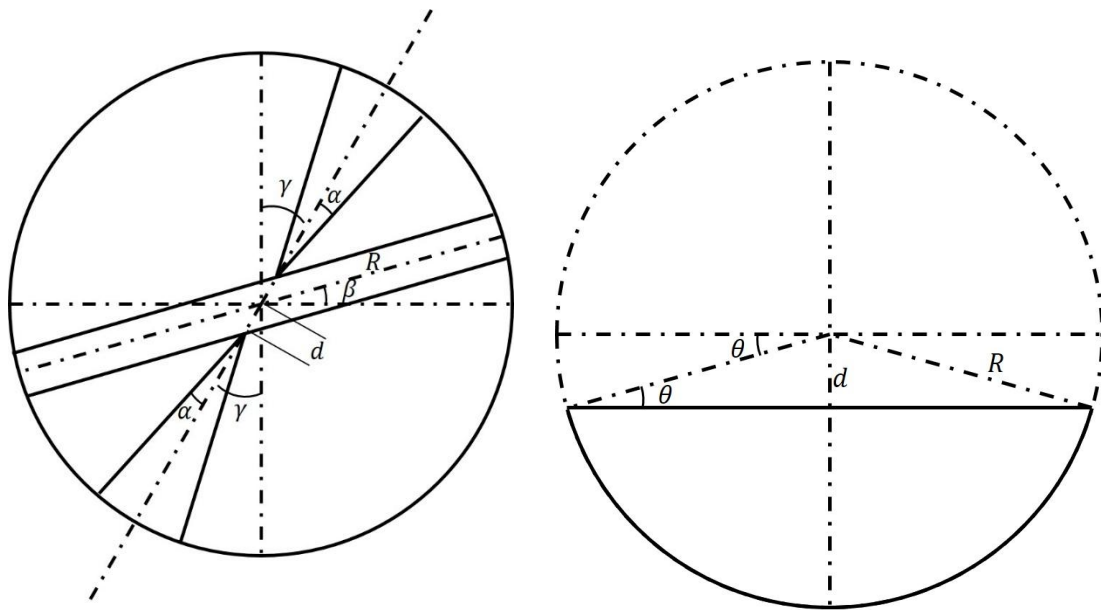


Fig. 8 (a) Front view at rotated angle  $\omega t = 0$  rad; (b) side view of the modified wedge.

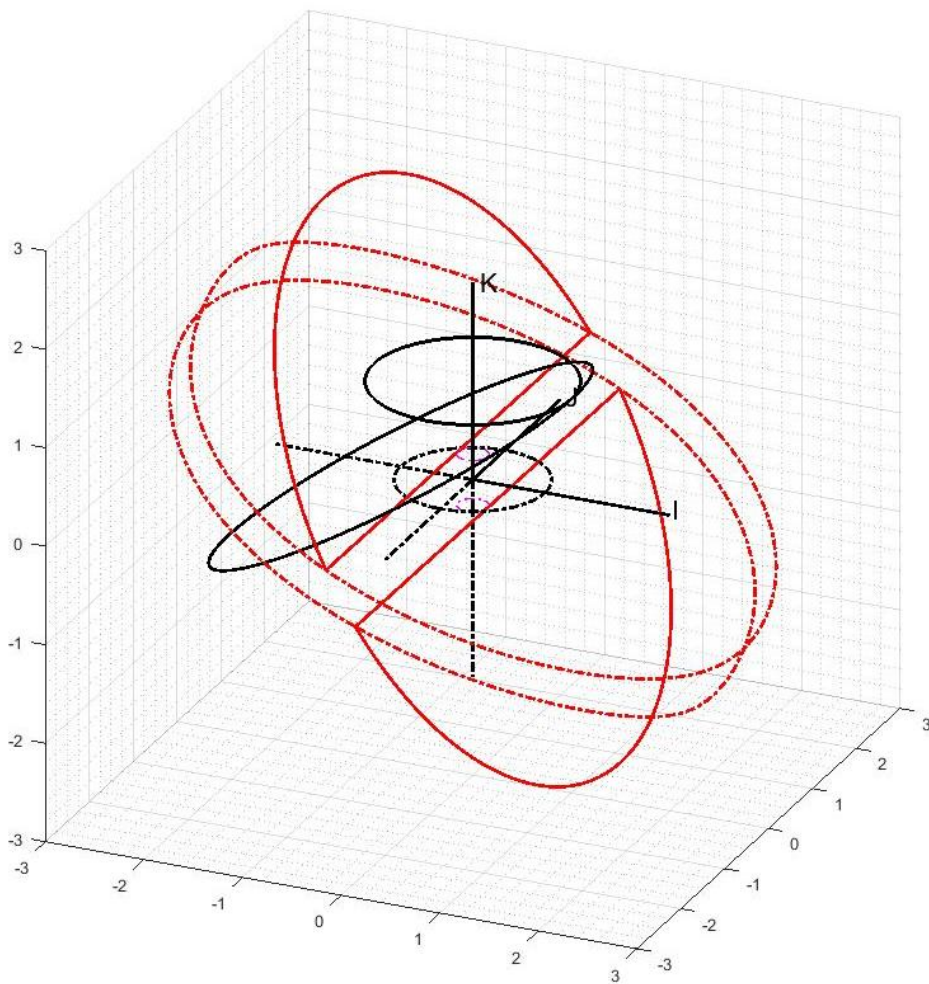
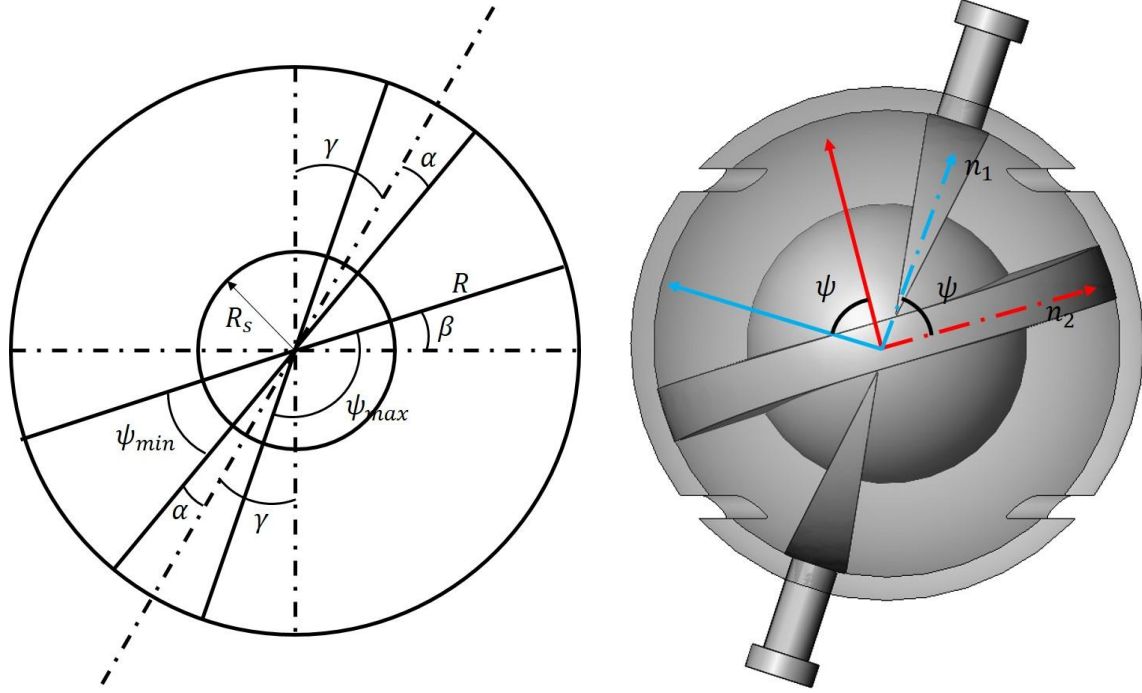


Fig. 9 Trajectories of the four tips on the modified wedge.



**Fig. 10** (a) Calculation of the angle between the infinite thin circular surface and the axial axis of the wedge; (b) normal directions of the infinite thin circular surface and the axial axis of the wedge.

where  $R_s$  is the radius of the middle sphere which contains the gear set.

To allow the TAH have the similar volume range as a real heart, the minimum volume ( $Ch1$  in Fig. 4a) and maximum volume ( $Ch2$  in Fig. 4a) are set to have the following relation:

$$\frac{V_{min}}{V_{max}} = \frac{\frac{\psi_{min}}{2\pi} \cdot \frac{4}{3}\pi(R^3 - R_s^3)}{\frac{\psi_{max}}{2\pi} \cdot \frac{4}{3}\pi(R^3 - R_s^3)} = \frac{\frac{\pi i}{2} - \alpha - \beta - \gamma}{\frac{\pi i}{2} - \alpha + \beta + \gamma} \quad (27)$$

$$= \frac{50 \text{ mL}}{130 \text{ mL}}$$

With Eq. (27) solved, we obtain  $0 < \alpha = \frac{\pi i}{2} -$

$\frac{9}{2}\beta < \beta$ . A solution set of

$(\alpha, \beta, R, R_s) = (9^\circ, 18^\circ, 50 \text{ mm}, 30 \text{ mm})$  gives a good result of  $V_{min} = 51.31 \text{ mL}$ ,  $V_{max} = 133.41 \text{ mL}$ , which are similar to the values of a real heart.

Since the chamber volume is a portion of a sphere, it is equivalent to calculate the angle between the ideal infinite thin circular plane and the axial axis of the wedge, which is the same angle as the one between

their normal directions, shown in Fig. 11.

$$\bar{n}_1 = s\beta\bar{I} + 0\bar{J} + c\beta\bar{K} \quad (28)$$

$$\bar{n}_2 = \bar{R} + [Rc0 \quad Rs0 \quad -h]R_3^{-1} \begin{bmatrix} \bar{I} \\ \bar{J} \\ \bar{K} \end{bmatrix} + hc\beta\bar{K} \quad (29)$$

$$\psi = \cos^{-1}\left(\frac{\bar{n}_1 \cdot \bar{n}_2}{|\bar{n}_1| \cdot |\bar{n}_2|}\right) \quad (30)$$

So the chamber volume can be calculated with Eqs. (26) and (28)-(30). The working principle of this 4-chamber version spherical gerotor is illustrated in Fig. 11. Fig. 12 plots the four varying chamber volumes against the rotated angle  $wt$ , where the rotating speed  $w$  is assumed to be constant here though it does not have to be.

#### 4. Discussion

Unlike those continuous flow TAHs or VADs which are non-positive displacement pumps, the proposed spherical gerotor TAH is a positive displacement pump, meaning a volumetric pump, the mean flow rate is determined by the rotating speed and the geometry displacement. If desired, good control

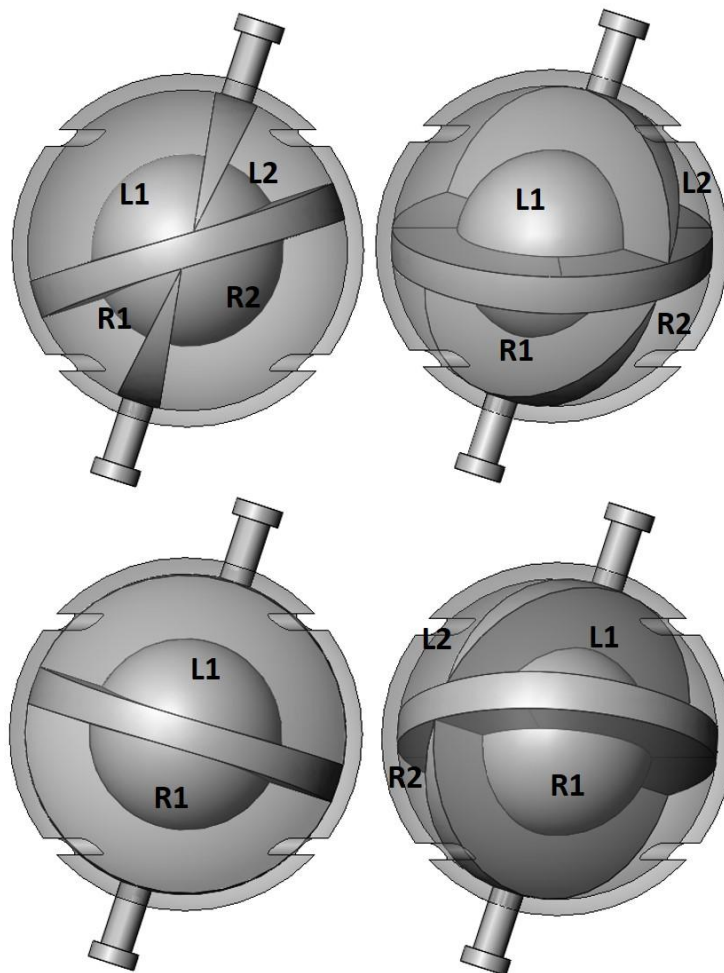


**Fig. 11 Working principle:** (a) rotated angle  $wt = 0 \text{ rad}$ , (b) rotated angle  $wt = \pi/4 \text{ rad}$ , (c) rotated angle  $wt = \pi/2 \text{ rad}$ , (d) rotated angle  $wt = 3\pi/2 \text{ rad}$ .

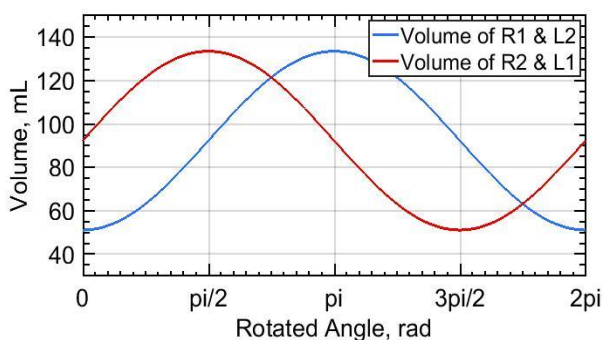


**Fig. 12 Chamber volume vs. rotated angle  $wt$ .**

algorithms can be applied to control the rotating speed to produce a physiological-friendly blood flow rate. Also, compared with those axial rotary TAH pumps, the blood shear stress by the proposed TAH itself is minimized theoretically by the low pump rotating

speed and low speed gradient. Most of the current MHVs are pivot mechanism based and they induce thrombus formation, which requires life long anti-coagulation. The usage of obturators proposed in Ref. [23] to replace those MHVs can be applied to our proposed design to achieve valveless property.

The inherent architectures of existing pulsatile flow TAHs (e.g. SynCardia, Carmat) pre-determine the bulky size of themselves. The proposed spherical gerotor TAH pump takes advantage of its own geometry characteristics to contain four variable chambers in one compact sphere, like the real one. Since the system degree of freedom (DoF) is reduced to one, only one servo motor, with necessary control circuits, is required to drive the whole TAH. Wireless

battery recharge can also be applicable. The main drawback of this architecture, though, is that since the DoF is reduced to one, the motions of the left side and right side are coupled together, unlike the real one.

## 5. Conclusion

This paper presents the design of a novel spherical total artificial heart (TAH) based on the concept of hydraulic gerotor pump. This spherical TAH features volumetric pumping mechanism, pulsatile flow generating and low blood shear. The fundamental working principle of the proposed spherical gerotor based TAH pump is presented and methods to derive the geometry shape of the spherical gerotor pump are described in details. An analytical model to calculate the chamber volume with respect to rotated angle is presented. Future work would include but not limit to (1) build the first prototype with Plexigals® made spherical part and brass made rotating disk and wedges; (2) demonstrate proof-of-principle with regard to showing the low device thrombogenicity of proposed TAH *in-silico* using Device Thrombogenicity Emulation (DTE) methodology [3, 4].

## Acknowledgement

This project is sponsored by the Center for Compact and Efficient Fluid Power (CCEFP) under NSF grant #0540834 with funding from the National Fluid Power Association (NFPA) Education and Technology Foundation. And the author would like to appreciate Dr. Ruchi Guo in Virginia Polytechnic Institute and State University for mathematical inspirations.

## References

- [1] Fraser, K. H., Zhang, T., Taskin, M. E., Griffith, B. P., and Wu, Z. J. 2012. "A Quantitative Comparison of Mechanical Blood Damage Parameters in Rotary Ventricular Assist Devices: Shear Stress, Exposure Time and Hemolysis Index." *Journal of Biomechanical Engineering* 134 (8): 081002.
- [2] Lloyd-Jones, D., Adams, R., Carnethon, M., De Simone, G., Ferguson, T. B., Flegal, K., Ford, E., Furie, K., Go, A., Greenlund, K., and Haase, N. 2009. "Heart Disease and Stroke Statistics—2009 Update." *Circulation* 119 (3): e21-e181.
- [3] Girdhar, G., Xenos, M., Alemu, Y., Chiu, W. C., Lynch, B. E., Jesty, J., Einav, S., Slepian, M. J., and Bluestein, D. 2012. "Device Thrombogenicity Emulation: A Novel Method for Optimizing Mechanical Circulatory Support Device Thromboresistance." *PLoS One* 7 (3): 32463.
- [4] Xenos, M., Girdhar, G., Alemu, Y., Jesty, J., Slepian, M., Einav, S., and Bluestein, D. 2010. "Device Thrombogenicity Emulator (DTE)—Design Optimization Methodology for Cardiovascular Devices: A Study in Two Bileaflet MHV Designs." *Journal of Biomechanics* 43 (12): 2400-9.
- [5] Goldfarb, S. B., Levvey, B. J., Edwards, L. B., Dipchand, A. I., Kucheryavaya, A. Y., Lund, L. H., Meiser, B., Rossano, J. W., Yusef, R. D., and Stehlik, J. 2016. "The Registry of the International Society for Heart and Lung Transplantation: Nineteenth Pediatric Lung and Heart–Lung Transplantation Report—2016; Focus Theme: Primary Diagnostic Indications for Transplant." *The Journal of Heart and Lung Transplantation* 35 (10): 1196-205.
- [6] Mozaffarian, D., Benjamin, E. J., Go, A. S., Arnett, D. K., Blaha, M. J., Cushman, M., De Ferranti, S., Després, J. P., Fullerton, H. J., Howard, V. J., and Huffman, M. D. 2015. "Heart Disease and Stroke Statistics—2015 Update: A Report from the American Heart Association." *Circulation* 131 (4): 29-322.
- [7] Schmitto, J. D., Zimpfer, D., Fiane, A. E., Larbalestier, R., Tsui, S., Jansz, P., Simon, A., Schueler, S., and Strueber, M. 2016. "Long-Term Support of Patients Receiving a Left Ventricular Assist Device for Advanced Heart Failure: A Follow-Up Analysis of the Registry to Evaluate the HeartWare Left Ventricular Assist System." *European Journal of Cardio-Thoracic Surgery* 50 (5): 834-8.
- [8] Heart Failure Society of America. 2010. "HFSA 2010 Comprehensive Heart Failure Practice Guideline." *J Card Fail* 16: e1-e194.
- [9] Kirklin, J. K., Naftel, D. C., Pagani, F. D., Kormos, R. L., Stevenson, L. W., Blume, E. D., Miller, M. A., Baldwin, J. T., and Young, J. B. 2014. "Sixth INTERMACS Annual Report: A 10,000-Patient Database." *The Journal of Heart and Lung Transplantation* 33 (6): 555-64.
- [10] Copeland, J. G., Arabia, F. A., Tsau, P. H., Nolan, P. E., McClellan, D., Smith, R. G., and Slepian, M. J. 2003. "Total Artificial Hearts: Bridge to Transplantation." *Cardiology Clinics* 21 (1): 101-13.
- [11] Letsou, G. V., Shah, N., Gregoric, I. D., Myers, T. J., Delgado, R., and Frazier, O. H. 2005. "Gastrointestinal

- Bleeding from Arteriovenous Malformations in Patients Supported by the Jarvik 2000 Axial-Flow Left Ventricular Assist Device.” *The Journal of Heart and Lung Transplantation* 24 (1): 105-9.
- [12] Eckman, P. M., and John, R. 2012. “Bleeding and Thrombosis in Patients with Continuous-Flow Ventricular Assist Devices.” *Circulation* 125 (24): 3038-47.
- [13] Crow, S., Chen, D., Milano, C., Thomas, W., Joyce, L., Piacentino, V., Sharma, R., Wu, J., Arepally, G., Bowles, D., and Rogers, J. 2010. “Acquired von Willebrand Syndrome in Continuous-Flow Ventricular Assist Device Recipients.” *The Annals of Thoracic Surgery* 90 (4): 1263-69.
- [14] Cowger, J., Pagani, F. D., Haft, J. W., Romano, M. A., Aaronson, K. D., and Kolias, T. J. 2010. “The Development of Aortic Insufficiency in Left Ventricular Assist Device-Supported Patients: Clinical Perspective.” *Circulation: Heart Failure* 3 (6): 668-74.
- [15] Soleimani, B., Haouzi, A., Manoskey, A., Stephenson, E. R., El-Banayosy, A., and Pae, W. E. 2012. “Development of Aortic Insufficiency in Patients Supported with Continuous Flow Left Ventricular Assist Devices.” *ASAIO Journal* 58 (4): 326-9.
- [16] Aggarwal, A., Raghuvir, R., Eryazici, P., Macaluso, G., Sharma, P., Blair, C., Tatoes, A. J., Pappas, P. S., and Bhat, G. 2013. “The Development of Aortic Insufficiency in Continuous-Flow Left Ventricular Assist Device-Supported Patients.” *The Annals of Thoracic Surgery* 95 (2): 493-8.
- [17] Muthiah, K., Robson, D., Macdonald, P. S., Keogh, A. M., Kotlyar, E., Granger, E., Dhital, K., Spratt, P., Jansz, P., and Hayward, C. S. 2013. “Thrombolysis for Suspected Intrapump Thrombosis in Patients with Continuous Flow Centrifugal Left Ventricular Assist Device.” *Artificial Organs* 37 (3): 313-8.
- [18] Bhamidipati, C. M., Ailawadi, G., Bergin, J., and Kern, J. A. 2010. “Early Thrombus in a HeartMate II Left Ventricular Assist Device: A Potential Cause of Hemolysis and Diagnostic Dilemma.” *The Journal of Thoracic and Cardiovascular Surgery* 140 (1): e7-8.
- [19] Borgi, J., Tsiouris, A., Hodari, A., Cogan, C. M., Paone, G., and Morgan, J. A. 2013. “Significance of Postoperative Acute Renal Failure after Continuous-Flow Left Ventricular Assist Device Implantation.” *The Annals of Thoracic Surgery* 95 (1): 163-9.
- [20] Patel, A. M., Adeseun, G. A., Ahmed, I., Mitter, N., Rame, J. E., and Rudnick, M. R. 2012. “Renal Failure in Patients with Left Ventricular Assist Devices.” *Clinical Journal of the American Society of Nephrology* pp. CJN-06210612.
- [21] Moazami, N., Dembitsky, W. P., Adamson, R., Steffen, R. J., Soltesz, E. G., Starling, R. C., and Fukamachi, K. 2015. “Does Pulsatility Matter in the Era of Continuous-Flow Blood Pumps?”
- [22] Yamane, T. 2016. “What Kinds of Artificial Hearts Are Available?” In *Mechanism of Artificial Heart*. Springer, Tokyo, pp. 3-12.
- [23] Tozzi, P., Maertens, A., Emery, J., Joseph, S., Kirsch, M., and Avellan, F. 2017. “An Original Valveless Artificial Heart Providing Pulsatile Flow Tested in Mock Circulatory Loops.” *The International Journal of Artificial Organs* 40 (12): 683-9.
- [24] Gerosa, G., Scuri, S., Iop, L., and Torregrossa, G. 2014. “Present and Future Perspectives on Total Artificial Hearts.” *Annals of Cardiothoracic Surgery* 3 (6): 595.
- [25] Cohrs, N. H., Petrou, A., Loepfe, M., Yliruka, M., Schumacher, C. M., Kohll, A. X., Starck, C. T., Schmid Daners, M., Meboldt, M., Falk, V., and Stark, W. J. 2017. “A Soft Total Artificial Heart—First Concept Evaluation on a Hybrid Mock Circulation.” *Artificial Organs* 41 (10): 948-58.
- [26] Wappenschmidt, J., Sonntag, S. J., Buesen, M., Gross-Hardt, S., Kaufmann, T., Schmitz-Rode, T., Autschbach, R., and Goetzenich, A. 2017. “Fluid Dynamics in Rotary Piston Blood Pumps.” *Annals of Biomedical Engineering* 45 (3): 554-66.